Journal of Solid State Chemistry **160,** 287–291 (2001)
doi:10.1006/jssc.2001.9260, available online at http://www.idealibrary.com on IDEAL®

# Consequence of the Metal-Atom Clustering on the Magnetic Properties in Vanadium Sulfide $V_5S_8$

H.-J. Koo, D.-K. Seo, and M.-H. Whangbo[1]

*Department of Chemistry, North Carolina State University, Raleigh, North Carolina 27695-8204*

Received March 15, 2001; in revised form May 11, 2001; accepted May 25, 2001

**On the basis of qualitative bonding considerations and tight-binding electronic band structure calculations, we examined how the unequal spin moment distribution is related to the metal-atom clustering in $V_5S_8$ and why $V_5S_8$ exhibits both localized and itinerant magnetic properties.** © 2001 Academic Press

## 1. INTRODUCTION

The crystal structure (1–5), physical properties (6–15) and electronic structure (16) of vanadium sulfide $V_5S_8$ have been studied for over three decades. $V_5S_8$ consists of $VS_2$ layers that are made up of edge-sharing $VS_6$ octahedra. In each $VS_2$ layer the vanadium atoms (i.e., V(2) and V(3)) form a cluster-pattern of "isolated diamonds" (Fig. 1a). The structure of $V_5S_8$ results when vanadium atoms (i.e., V(1)) are introduced into the octahedral sites between adjacent $VS_2$ layers such that all the $V_4$ diamonds of adjacent layers are linked via the V(3)–V(1)–V(3) bridges as depicted in Fig. 1b. $V_5S_8$ is metallic at all temperatures (7), exhibits a Curie–Weiss paramagnetic behavior above 35 K (10), and orders antiferromagnetically below 35 K (12). Only the V(1) sites carry spin magnetic moments (6, 8, 12), and the effective moments in the paramagnetic state are $\sim 2.3\ \mu_B$ per V(1) (6, 9, 10). NMR studies (11, 12) suggested that the ordered moments in the antiferromagnetic state are $0.22\ \mu_B$ per V(1), whereas the neutron diffraction study (13) indicated a much larger value (up to $1.50\ \mu_B$ per V(1)). This discrepancy was resolved by the recent magnetization study (15), which found the ordered moments to be $1.50\ \mu_B$ per V(1) (i.e., 1.5 unpaired electrons on each V(1)). For $V_5Se_8$, which is isostructural and isoelectronic with $V_5S_8$, this study found a smaller ordered magnetic moment on each V(1) (i.e., $1.2\ \mu_B$). It has been pointed out that the magnetic properties of $V_5S_8$ are explained by considering both localized and itinerant magnetism (14).

[1]To whom correspondence should be addressed.

So far there has been one report of electronic band structure study for $V_5S_8$. Knecht *et al.* (16) carried out spin-polarized electronic band structure calculations using the linear muffin-tin orbital method (LMTO) (17) to find that the Stoner criterion for spontaneous formation of a spin magnetic moment is fulfilled locally only for the V(1) site, but not for the V(2) and V(3) sites, and that the antiferromagnetic state of $V_5S_8$ is more stable than the metallic or ferromagnetic state. Their analysis also indicated that the spin magnetic moment of V(1) for the antiferromagnetic state persists above the Néel temperature hence giving rise to a Curie–Weiss paramagnetic behavior. These findings of Knecht *et al.* are in agreement with the experiment. Nevertheless, up to now, it is not well understood how the unequal spin moment distribution is related to the metal-atom clustering in $V_5S_8$ and why $V_5S_8$ exhibits both localized and itinerant magnetic properties. In the present work, we probe these questions by analyzing how the metal-atom clustering in $V_5S_8$ affects its *d*-block band structure on the basis of both qualitative metal-metal bonding considerations and tight binding electronic structure calculations for $V_5S_8$ using the extended Hückel method (18, 19). The atomic parameters used for the present calculations are summarized in Table 1.

## 2. NATURE OF THE *d*-BLOCK ELECTRONIC BAND STRUCTURE AROUND THE FERMI LEVEL

The plot of the density of states (DOS) calculated for $V_5S_8$ is presented in Fig. 2a, where the solid line represents the total DOS and the dotted line represents the partial DOS for the V 3*d* orbitals. The Fermi level lies at a sharp DOS peak of the *d*-block bands. The contribution of each nonequivalent vanadium atom to the sharp DOS peak at the Fermi level is shown in Fig. 2b, which reveals that the V(1) atom contribution dominates. The contribution of each vanadium atom to the DOS at the Fermi level, $N(E_f)$, decreases in the order $V(1) > V(3) > V(2)$ (i.e., $N(E_f) = 4.15$, 1.67 and 0.93 states/atom for V(1), V(3), and V(2), respectively). Thus with the Stoner exchange-



0022-4596/01 $35.00

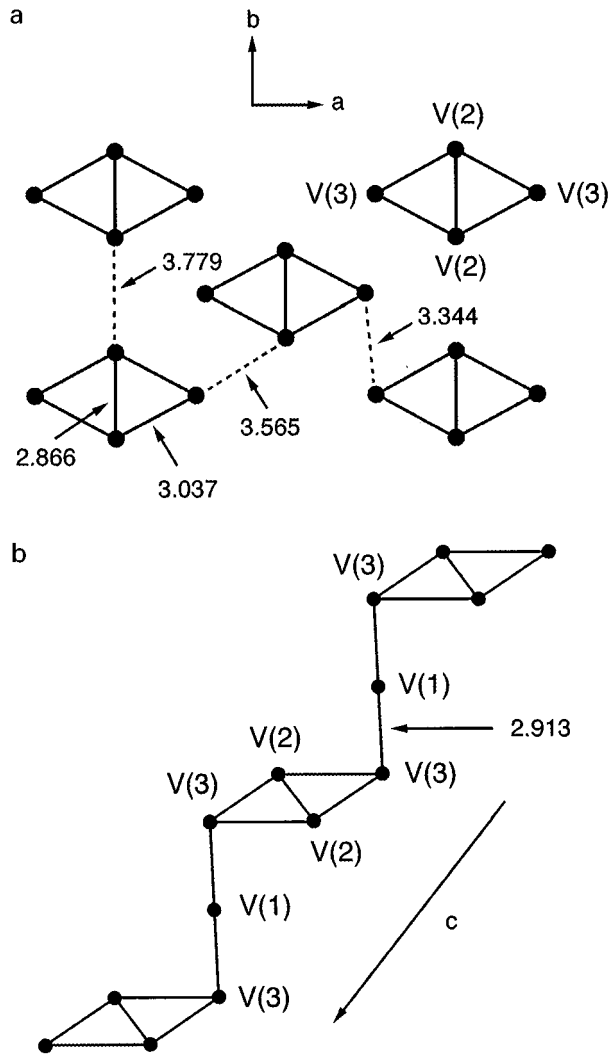


**FIG. 1.** (a) Isolated diamond pattern of metal-atom clustering in the $VS_2$ layers of $V_5S_8$. (b) Linking between the $V_4$ "diamonds" of $V_5S_8$ via V(3)–V(1)–V(3) bridges. The heavy dots refer to vanadium atoms, and the metal–metal distances are given in Å.

correlation integral $I = 0.35$ eV for pure V (20), the Stoner enhancement factor $S = 1/[1 - N(E_f)]$ is calculated to be negative only for V(1), i.e., the Stoner criterion for spontaneous formation of a spin magnetic moment is fulfilled only for V(1). The V(1) atom contribution to the sharp DOS peak at the Fermi level is decomposed into three types of *d*-orbitals in Fig. 2c (i.e., $x^2 - y^2$ and $xy$; $xz$ and $yz$; $z^2$ under the coordinate scheme in which the $xy$ plane is taken to be parallel to the $VS_2$ layers), which clearly shows that the in-plane *d* orbitals (i.e., $x^2 - y^2$ and $xy$) contribute most. All these findings of the present calculations are essentially the same as those obtained by Knecht *et al.* from LMTO calculations. We note that the $xz/yz$ orbital contribution to the sharp DOS peak at the Fermi level is only slightly smaller than is the $x^2 - y^2/xy$ orbital contribution while the $z^2$ orbital contribution is negligible.

**TABLE 1**

**Exponents $\zeta_i$ and Valence Shell Ionization Potentials $H_{ii}$ of Slater-Type Orbitals $\chi_i$ Used for Extended Hückel Tight-Binding Calculations**[a]

| Atom | $\chi_i$ | $H_{ii}$ (eV) | $\zeta_i$ | $c_1^b$ | $\zeta_i'$ | $c_2^b$ |
|---|---|---|---|---|---|---|
| V | 4*s* | − 8.81 | 1.300 | 1.0 | | |
| V | 4*p* | − 5.52 | 1.300 | 1.0 | | |
| V | 3*d* | − 11.0 | 4.750 | 0.4755 | 1.700 | 0.7052 |
| S | 2*s* | − 20.0 | 2.122 | 1.0 | | |
| S | 2*p* | − 13.3 | 1.827 | 1.0 | | |

[a] $H_{ii}$'s are the diagonal matrix elements $\langle\chi_i|H^{eff}|\chi_i\rangle$, where $H^{eff}$ is the effective Hamiltonian. In our calculations of the off-diagonal matrix elements $H^{eff} = \langle\chi_i|H^{eff}|\chi_j\rangle$, the weighted formula was used. See J. Ammeter, H.-B. Bürgi, J. Thibeault, and R. Hoffmann, *J. Am. Chem. Soc.* **100,** 3686 (1978).

[b] Contraction coefficients used in the double-zeta Slater-type orbital.

## 3. METAL-ATOM CLUSTERING AND *d*-ELECTRON COUNTING

In this section we examine why the Fermi level of $V_5S_8$ lies at a sharp DOS peak of its *d*-block bands and why the vanadium atom contribution to this DOS peak decreases in the order V(1) > V(3) > V(2). To answer these questions, we first consider how the metal-atom clustering pattern of $V_5S_8$ can be understood from the viewpoint of qualitative metal-metal bonding considerations. $MQ_2$ ($M$ = transition metal, $Q$ = O, S, Se, Te) layers made up of edge-sharing $MQ_6$ octahedra exhibit various metal-atom clustering patterns depending on the *d*-electron count of their transition metal cations (21, 22). As depicted in Fig. 3a, the $t_{2g}$ orbitals of an $MQ_6$ octahedron are contained in the three different equatorial planes. For two adjacent edge-sharing octahedra, the interactions between the two $t_{2g}$ orbitals contained in the common equatorial plane lead to sigma-bonding and sigma-antibonding ($\sigma$ and $\sigma^*$, respectively) levels (Fig. 3b). In principle, each $MQ_6$ octahedron can form three different sets of $\sigma$ and $\sigma^*$ levels using its $t_{2g}$ orbitals. When such a $\sigma$-level is filled with two *d* electrons, a two-center–two-electron ($2c$–$2e$) bond results. The "zig-zag chains" or "isolated trimers" of the $MQ_2$ layers with $d^2$ ions as well as the "diamond-chains" with $d^3$ ions are all explained in terms of $2c$–$2e$ bonds (20, 21).

Let us now discuss how the metal-atom clustering pattern of $V_5S_8$ can be explained in terms of metal–metal bonding interactions. First, it is noticed that in each V(3)–V(1)–V(3) bridge the $V(1)S_6$ octahedron share its two *trans* faces with the two $V(3)S_6$ octahedra, and that $V_5S_8$ has nine *d* electrons per formula unit due to the oxidation state $S^{2-}$. To simplify our discussion, it will be assumed that there is one unpaired

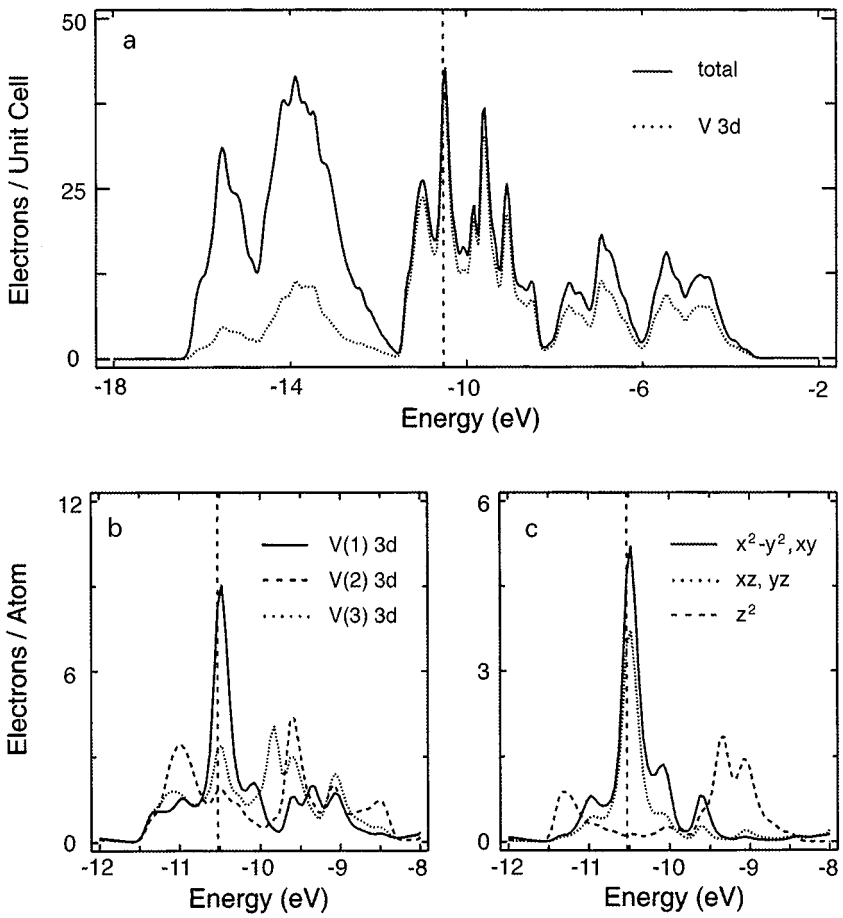


**FIG. 2.** (a) DOS plots calculated for $V_5S_8$, where the vertical dashed line represents the Fermi level. (b) Contribution of each nonequivalent vanadium atom to the DOS around the Fermi level. (c) Contribution of the *d* orbitals of V(1) to the DOS around the Fermi level.

electron on each V(1). This means that $V_5S_8$ uses eight *d* electrons per formula unit to form seven metal–metal bonds, i.e., one V(2)–V(2), four V(2)–V(3), and two V(1)–V(3) bonds. Since the V(2)–V(2) bond is short (2.866 Å), it is reasonable to regard the V(2)–V(2) bond as a 2c–2e bond (Fig. 4). This leaves six *d* electrons to form the remaining six metal–metal bonds. The V(2)–V(3) and V(1)–V(3) bonds (3.037 and 2.913 Å, respectively) are not short enough to be a 2c–2e bond. If the V(2)–V(3) and V(1)–V(3) bonds each have the strength of a two-center one-electron bond (Fig. 4), then precisely six *d* electrons are needed to form four V(2)–V(3) and two V(1)–V(3) bonds. This suggests that each V(3)–V(1)–V(3) bridge is a three-center–two-electron (3*c*–2*e*) bond, while the $V_4$ rhombus consisting of four V(2)–V(3) bonds has two four-center–two-electron (4*c*–2*e*) bonds. Since the number of electrons in a two-center covalent bond is equally shared between the two centers, the qualitative *d* electron counting presented in Fig. 4 suggests that the V(1), V(2), and V(3) atoms possess 2, 2, 1.5 *d* electrons, respectively, and hence that the oxidation states of V(1), V(2), and V(3) are + 3, + 3, and + 3.5, respectively. In the following, we probe further implications of this qualitative *d* electron counting from the viewpoint of metal–metal interactions involving their $t_{2g}$ orbitals.

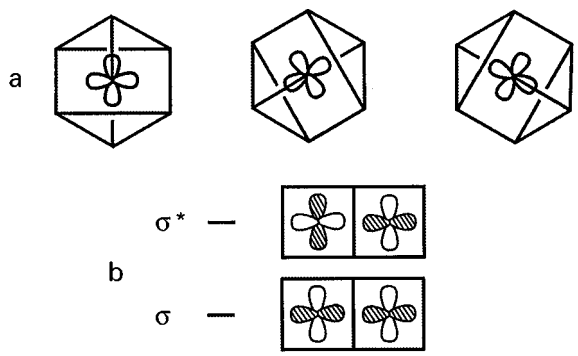


**FIG. 3.** (a) Three equatorial planes of a $VS_6$ octahedron containing the $t_{2g}$ orbitals. (b) Interactions between two adjacent $t_{2g}$ orbitals leading to sigma-bonding and sigma-antibonding levels.

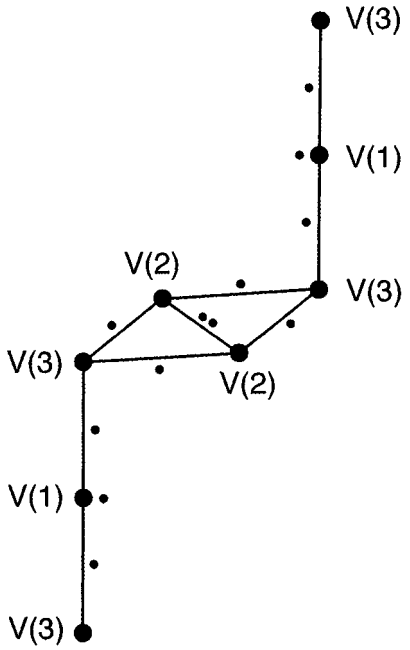


**FIG. 4.** Schematic representation of a $V_8S_{28}$ cluster consisting of one $V_4$ diamond and two V(3)–V(1)–V(3) bridges. For simplicity, only the metal atom arrangement is shown as heavy dots. The small dots represent $d$ electrons present on the V(1) atoms and in the V(2)–V(2), V(2)–V(3), and V(1)–V(3) metal-metal bonds.

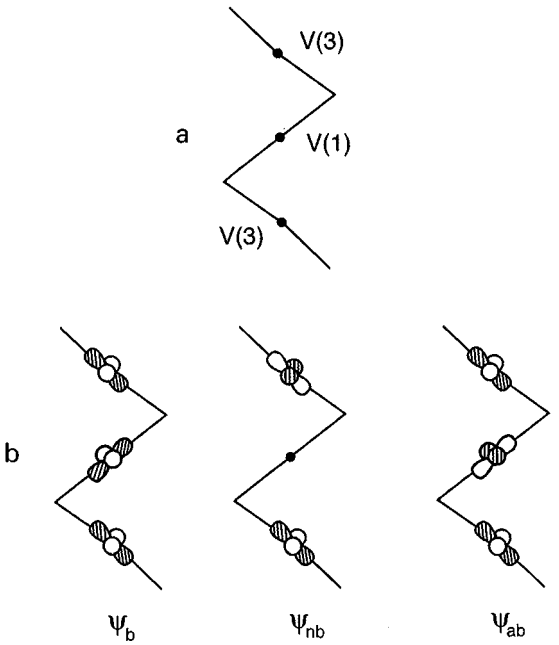


**FIG. 5.** (a) Schematic projection view of a V(3)–V(1)–V(3) bridge. Each line segment containing a metal atom represents the equatorial plane containing its $t_{2g}$ orbital. (b) Bonding, nonbonding, and antibonding levels ($\psi_b$, $\psi_{nb}$, and $\psi_{ab}$, respectively) of a V(3)–V(1)–V(3) bridge resulting from the three $t_{2g}$ orbitals.

The metal-atom clustering pattern of Fig. 1b indicates that each V(2) atom utilizes all three $t_{2g}$ orbitals, but each V(3) atom utilizes two $t_{2g}$ orbitals, to have metal–metal interactions within the $VS_2$ layer. From the viewpoint of two-center metal–metal interaction, each V(2)–V(3) bond uses two $t_{2g}$ orbitals (Fig. 3b) so that altogether eight $t_{2g}$ orbitals are involved in describing the metal–metal interactions of the four V(2)–V(3) bonds in a $V_4$ diamond. Let us assume that due to the weak metal–metal interactions, the linear combinations of these eight orbitals form only two four-center bonding levels (rather than four two-center bonding levels). When these bonding levels are each doubly occupied, we obtain two $4c$–$2e$ bonds that provide in average one electron per V(2)–V(3) bond (Fig. 4). Then six $d$ electrons are necessary to account for one V(2)–V(2) and four V(2)–V(3) bonds of each $V_4$ diamond. This leaves three $d$ electrons per formula unit to describe the metal–metal bonding of each V(3)–V(1)–V(3) bridge (Fig. 4).

Each V(3) atom has one $t_{2g}$ orbital not used in forming the $V_4$ diamond. In each V(3)–V(1)–V(3) bridge such $t_{2g}$ orbitals of the two V(3) atoms can interact with one of the three $t_{2g}$ orbitals of V(1). At this point one may wonder what set of $t_{2g}$ orbitals to employ for the V(1)$S_6$ octahedron. The $t_{2g}$ orbitals of Fig. 3a constitute one set. When linearly combined, these orbitals generate an alternative set in which one member is represented primarily by the $z^2$ orbital aligned along the threefold rotational axis (23). For our discussion, however, it is irrelevant which set we use (see below). For simplicity, let us employ the $t_{2g}$ orbitals of Fig. 3a. Then, the three $t_{2g}$ orbitals of a V(3)–V(1)–V(3) bridge making metal–metal interactions are contained in the equatorial planes shown in Fig. 5a, where the planes are projected as line segments. The linear combinations of the three orbitals contained in these equatorial planes produce the bonding, nonbonding, and antibonding levels ($\psi_b$, $\psi_{nb}$, and $\psi_{ab}$, respectively) of the V(3)–V(1)–V(3) bridge (Fig. 5b). If we use the alternative set of $t_{2g}$ orbitals for V(1), as mentioned above, it is necessary to replace the $t_{2g}$ orbital of V(1) in $\psi_b$ and $\psi_{ab}$ with the $z^2$ orbital of V(1). By symmetry, the $z^2$ orbital of V(1) cannot contribute to the nonbonding level $\psi_{nb}$. In short, the use of the alternative set of $t_{2g}$ orbitals for V(1) does not change the bonding picture. The two $t_{2g}$ orbitals of the V(1)$S_6$ octahedron not making the metal–metal interactions of a V(3)–V(1)–V(3) bridge are left over as nonbonding levels, which we will refer to as $\Phi_{nb}$ and $\Phi'_{nb}$. When the bonding level $\psi_b$ is doubly occupied, each V(3)–V(1)–V(3) linkage becomes a $3c$–$2e$ bond. Consequently, $V_5S_8$ has one electron per formula unit to fill the three nonbonding levels $\psi_{nb}$, $\Phi_{nb}$, and $\Phi'_{nb}$.

To confirm the correctness of the above $d$ electron counting scheme and its implications, we performed molecular orbital calculations for the $V_8S_{28}$ cluster that consists of a $V_4$ diamond and two V(3)–V(1)–V(3) bridges (Fig. 4). This cluster has four V(3) atoms. Two of them are part of the

$V_4$ diamond, while the remaining clusters are part of other $V_4$ diamonds truncated away in our calculations. As anticipated from the counting scheme, our calculations show that the $V_8S_{28}$ cluster has five bonding levels resulting from one $2c$–$2e$, two $4c$–$2e$, and two $3c$–$2e$ bonding levels as well as six nonbonding levels resulting from two $\psi_{nb}$, two $\Phi_{nb}$, and two $\Phi'_{nb}$ levels. The $V_8S_{28}$ cluster also has four more nonbonding levels, because each of the two terminal V(3) atoms do not use two $t_{2g}$ orbitals due to the truncation.

## 4. DISCUSSION

The observation that $V_5S_8$ has one electron to fill the three nonbonding levels $\psi_{nb}$, $\Phi_{nb}$, and $\Phi'_{nb}$ per formula unit has important implications. These levels constitute the highest occupied $d$-block bands of $V_5S_8$. The latter should give rise to a sharp DOS peak at the Fermi level, because the nonbonding levels $\Phi_{nb}$ and $\Phi'_{nb}$ of each $V(1)S_6$ octahedron have contributions only from the V(1) atom and because the V(1) atoms are well separated from each other in $V_5S_8$. By symmetry, the nonbonding level $\psi_{nb}$ of each V(3)–V(1)–V(3) bridge has contributions only from the V(3) atoms. The interaction between the $\psi_{nb}$ levels in $V_5S_8$ would not vanish because the $t_{2g}$ orbitals of adjacent V(3) atoms within each $VS_2$ layer can interact weakly either directly or indirectly through a V(2) atom (Fig. 1a), and hence give rise to a slight spreading of the sharp DOS peak at the Fermi level and nonzero contribution of the V(2) atom to $N(E_f)$. To a first approximation, the three nonbonding levels $\psi_{nb}$, $\Phi_{nb}$, and $\Phi'_{nb}$ are equally populated. This explains why the vanadium atom contribution to the sharp DOS peak at the Fermi level varies in the order V(1) > V(3) > V(2). It is most likely that the localized magnetic character of $V_5S_8$ stems from the two nonbonding $t_{2g}$ levels ($\Phi_{nb}$ and $\Phi'_{nb}$) of the $V(1)S_6$ octahedra at the Fermi level, and the itinerant magnetic character of $V_5S_8$ from the nonbonding levels ($\psi_{nb}$) of the V(3)–V(1)–V(3) bridges at the Fermi level.

## 5. CONCLUDING REMARKS

The present work shows that the unequal spin moment distribution and the occurrence of both localized and itinerant magnetisms in $V_5S_8$ are intimately related to the metal–atom clustering pattern in $V_5S_8$. Qualitative considerations of the metal–metal bonding interactions indicate that the metal-atom clustering requires eight $d$ electrons per formula unit, thereby leaving one $d$ electron per formula unit to fill the one nonbonding level of the V(3)–V(1)–V(3) bridge and two nonbonding $t_{2g}$ levels of the $V(1)S_6$ octahedron. The latter provides a natural explanation for why both localized and itinerant magnetisms exist in $V_5S_8$.

## ACKNOWLEDGMENT

Work at North Carolina State University was supported by the Office of Basic Energy Sciences, Division of Materials Sciences, U.S. Department of Energy, under Grant DE-FG05-86ER45259.

## REFERENCES

1. S. Brunie and M. Chevreton, *Cont. Rend.* **258,** 5847 (1964).
2. F. Gronvold, H. Haraldsen, B. Pedersen, and T. Tufte, *Rev. Chim. Miner.* **6,** 251 (1969).
3. A. B. de Vries and F. Jellinek, *Rev. Chim. Miner.* **11,** 624 (1974).
4. I. Kawada, M. Nakano-Onoda, M. Ishii, M. Saeki, and M. Nakahira, *J. Solid State Chem.* **15,** 246 (1975).
5. W. Bensch and J. Koy, *Inorg. Chim. Acta* **206,** 221 (1993).
6. A. B. de Vries and C. Haas, *J. Phys. Chem. Solids* **34,** 651 (1973).
7. H. Nozaki, Y. Ishizawa, M. Saeki, and M. Nakahira, *Phys. Lett. A* **54,** 29 (1975).
8. B. G. Silbernagel, R. B. Levy, and F. R. Gamble, *Phys. Rev. B* **11,** 4563 (1975).
9. H. Nishihara, H. Yasuoka, Y. Oka, K. Kosuge, and S. Kachi, *J. Phys. Soc. Jpn.* **42,** 787 (1977).
10. H. Nozaki, M. Umehara, Y. Ishizawa, M. Saeki, T. Mizoguchi, and M. Nakahira, *J. Phys. Chem. Solids*, **39,** 851 (1978).
11. Y. Kitaoka, H. Yasuoka, Y Oka, K. Kosuge, and S. Kachi, *J. Phys. Soc. Jpn.* **46,** 1381 (1979).
12. Y. Kitaoka and H. Yasuoka, *J. Phys. Soc. Jpn.* **48,** 1949 (1980).
13. S. Funahashi, H. Nozaki, and I. Kawada, *J. Phys. Chem. Solids* **42,** 1009 (1981).
14. A. Fujimori, M. Saeki, and H. Nozaki, *Phys. Rev. B* **44,** 163 (1991).
15. M. Naknishi, K. Yoshimura, K. Kosuge, T. Goto, T. Fujii, and J. Takada, *J. Magn. Magn. Mater.* **221,** 301 (2000).
16. K. Knecht, H. Ebert, and W. Bensch, *J. Phys.: Condens. Matter* **10,** 9455 (1998).
17. O. K. Anderson and O. Jepsen, *Phys. Rev. Lett.* **53,** 2571 (1984).
18. M.-H. Whangbo and R. Hoffmann, *J. Am. Chem. Soc.* **100,** 6397 (1978).
19. Our calculations were carried out by employing the *CAESAR* program package (J. Ren, W. Liang, and M.-H. Whangbo, "Crystal and Electronic Structure Analysis Using CAESAR," 1998, http://www.PrimeC.com).
20. J. F. Janak, *Phys. Rev. B* **16,** 255 (1977).
21. M.-H. Whangbo and E. Canadell, *J. Am. Chem. Soc.* **114,** 9587 (1992), and the references cited therein.
22. C. Rovira and M.-H. Whangbo, *Inorg. Chem.* **32,** 4094 (1993).
23. M.-H. Whangbo, M. J. Foshee, and R. Hoffmann, *Inorg. Chem.* **19,** 1723 (1980).